Preprint, Institute of Mathematics, AS CR, Prague. 2010-1-15

FULLY COMPUTABLE ROBUST A POSTERIORI ERROR BOUNDS FOR SINGULARLY PERTURBED REACTION–DIFFUSION PROBLEMS

MARK AINSWORTH AND TOMÁŠ VEJCHODSKÝ

Abstract. A procedure for the construction of robust, upper bounds for the error in the finite element approximation of singularly perturbed reaction diffusion problems was presented in [2] which entailed the solution of an infinite dimensional local boundary value problem. It is not possible to solve this problem exactly and this fact was recognised in the above work where it was indicated that the limitation would be addressed in a subsequent article. We view the present work as fulfilling that promise and as completing the investigation begun in [2] by removing the obligation to solve a local problem exactly. The resulting new estimator is indeed fully computable and the first to provide fully computable, robust upper bounds in the setting of singularly perturbed problems discretised by the finite element method.

Dedicated to Professor Ivo Babuška on the occasion of his 85th birthday.

1. Introduction

Consider the Dirichlet problem

$$-\Delta u + \kappa^2 u = f \text{ in } \Omega; \quad u = 0 \text{ on } \partial\Omega \tag{1}$$

where $\Omega \subset \mathbb{R}^2$ is a polygonal domain with boundary $\partial\Omega$ and κ is a non-negative constant. If $\kappa \gg 1$, then this problem is sometimes referred to as a singularly perturbed reaction–diffusion problem [10]. Methods that are entirely satisfactory for the approximate solution of unperturbed problems, i.e. $\kappa = \mathcal{O}(1)$, are frequently found wanting in the singularly perturbed case, i.e. $\kappa \gg 1$, in the sense that their performance degenerates as κ grows [10]. A method whose performance does not degenerate with κ is said to be *robust*.

The numerical approximation of singularly perturbed problems is frustrated by the fact that the true solutions of such problems generally feature sharp boundary layers, in addition to the usual corner and edge singularities present in elliptic problems. One way in which to combat these features is to use an adaptive finite element methods whereby elements are selectively refined where

1991 *Mathematics Subject Classification.* Primary 65N15. Secondary 65N30, 65J15.

Key words and phrases. Finite element analysis. A posteriori error estimate. Singularly perturbed problems. Boundary layers.

Date: January 15, 2010.

Partial support for M.A. from the Engineering and Physical Sciences Research Council under grant GR/S35103 and the support for T.V. from the Czech Science Foundation, from the Grant Agency of the Academy of Sciences, and from the Academy of Sciences of the Czech Republic, projects No. 102/07/0496, No. IAA100760702, and the institutional research plan No. AV0Z10190503 are gratefully acknowledged.

the solution is poorly resolved. The convergence of adaptive algorithms was first investigated by Dörfler [5], subsequently refined by Morin et al. [7] and the optimality of adaptive finite element methods was established by Stevenson [11]. A key ingredient in an adaptive finite element algorithm is the availability of a robust a posteriori error indicator η_K for the error in energy measured over an individual element K. The analysis of adaptive methods typically hinges on two key properties of the indicator. Firstly, the sums of the local indicators should provide a reliable upper bound for the total error $\|\!|e|\!\|$ measured in the energy norm, in the sense that there exists a positive constant C which is *independent of any mesh size and the parameter* κ such that

$$\|\!|e|\!\|^2 \leq C\eta^2 = C\sum_{K\in\mathcal{P}} \eta_K^2 \tag{2}$$

where $\mathcal{P}$ denotes the elements in the finite element partitioning of the domain Ω. Secondly, the estimator should be efficient in the sense that there exists a positive constant c, again *independent of any mesh size and the parameter* κ, such that

$$c\eta_K^2 \leq \|\!|e|\!\|_{\widetilde{K}}^2 \tag{3}$$

where $\widetilde{K}$ denotes the patch consisting of the element K together with neighbouring elements sharing a common node with the element K. If the elements satisfy the usual shape regularity condition, then by summing the latter estimate over all elements we see that the estimator provides two-sided bounds on the error

$$\frac{c}{m}\eta^2 \leq \|\!|e|\!\|^2 \leq C\eta^2$$

where m denotes the largest number of elements in any of the patches $\widetilde{K}$. Explicit a posteriori error indicators for (1) were first derived by Verfürth [12] and shown to provide robust two-sided estimates of the form (2) and (3).

Estimates (2) and (3) are sufficient to guarantee robust convergence of the adaptive algorithm. However, the indicator is often called upon to provide *a stopping criterion for the adaptive procedure* for which knowledge of the actual value of the constant C appearing in the upper bound is required. Ideally, we would like to have a fully computable upper bound of the form

$$\|\!|e|\!\|^2 \leq \eta = \sum_{K\in\mathcal{P}} \eta_K^2. \tag{4}$$

If the indicator η is known to provide an estimate for the error of this type, then we shall say that η is an a posteriori error estimator.

Our objective in the present work is to derive a fully computable, robust local a posteriori error estimators $\{\eta_K : K \in \mathcal{P}\}$ which together provide a true upper bound of the form (4) and, in addition, provide a robust local lower bound of the form (3) with a generic (unknown) positive constant c that is nevertheless independent of any mesh size and the parameter κ. Such an estimator would be suitable for both driving an adaptive refinement procedure and providing a quantitative, guaranteed stopping criterion for the algorithm.

Ainsworth and Babuška [2] derived implicit a posteriori error estimators for (1) that provide a robust local lower bound (3) and a guaranteed upper

bound (4). However, the estimator defined in [2] is based on the assumption that a local boundary value problem of the form (1) is solved *exactly* over each element K. The obligation to solve a local problem exactly means that the estimator in [2] is, strictly speaking, not actually fully computable. Of course, this limitation was already recognised by [2] where it was indicated that the issue would be fully addressed in a subsequent article. We view the present work as fulfilling that promise and, as such, completing the investigation begun in [2] by removing the obligation to solve a local problem exactly. The resulting new estimator is indeed fully computable and is the first to provide fully computable, robust upper bounds in the setting of finite element discretisation of singularly perturbed problems.

The challenge laid down in [2] was taken up by Grosman [6] who introduced a finite dimensional approximation for the local boundary value problem and showed that, up to unknown constants, the norm of the solution of the finite dimensional approximation is equivalent to that of the solution of the infinite dimensional problem. Unfortunately, the values of the constants could not be established. Moreover, numerical examples presented in [6] show that the resulting indicator fails to preserve the guaranteed upper bound property of the estimator presented in [2] and as such falls short of meeting the challenge. A computable upper bound for problem (1) discretised using a cell-centred finite volume method was presented by Cheddadi et al. [4] based on the use of an associated dual mesh.

The remainder of this paper is organized as follows. The basic assumptions and construction of the a posteriori error estimator are presented in the next three sections, followed by a section containing illustrations of the behaviour of the estimator in particular cases. The analysis of the estimator and proofs of the estimates conclude the paper.

2. Finite Element Approximation

2.1. **Assumptions.** We consider a family of partitions $\{\mathcal{P}\}$ of the domain Ω into the union of non-overlapping, triangular elements such that the non-empty intersection of a distinct pair of elements is a single common node or single common edge. We denote the diameter of an element K by h_K and let $\boldsymbol{x}_K$ and ρ_K denote the *incentre* and the *inradius* of element K, i.e. the centre and the radius of the largest ball contained within K. The family of partitions is assumed to be regular so that the bound

$$\max_{K\in\mathcal{P}} \frac{h_K}{\rho_K} \leq C$$

where C is a positive constant, holds uniformly over the family. The patch consisting of an element K and its neighbours is denoted by

$$\widetilde{K} = \operatorname{int}\left\{\bigcup \overline{K'} : \overline{K'} \cap \overline{K} \text{ is non-empty}\right\}.$$

Thanks to the regularity assumption on the partitions, the number of elements in any such patch is uniformly bounded over the family as is the number of patches containing a particular element. Moreover, within each patch $\widetilde{K}$, a local quasi-uniformity condition $ch_K \leq h_{K'} \leq Ch_K$ holds for positive constants c and

C uniformly over the whole family of meshes. Similarly, the shape regularity of the elements means that there exists a positive constant $\mathcal{C}_0$ such that

$$\frac{1}{\mathcal{C}_0}\rho_K \leq \rho_{K'} \leq \mathcal{C}_0\rho_K \tag{5}$$

holds for all elements K' contained within the patch $\widetilde{K}$, where $\mathcal{C}_0$ is again uniformly bounded over the entire family of partitions. These conditions are sufficiently mild to permit the use of highly graded meshes such as those typically produced by an adaptive solution algorithm but preclude the use of anisotropic elements.

2.2. **Finite Element Approximation.** Let $X_{\mathcal{P}}$ denote the set of continuous, piecewise affine functions relative to the partition $\mathcal{P}$, and define the finite element subspace $V_{\mathcal{P}} = X_{\mathcal{P}} \cap H^1_0(\Omega)$. We approximate the solution of (1) by seeking $\mathrm{u}_{\mathcal{P}} \in V_{\mathcal{P}}$ such that

$$\mathcal{B}(\mathrm{u}_{\mathcal{P}}, v) = \mathcal{F}(v) \quad \forall v \in V_{\mathcal{P}} \tag{6}$$

where $\mathcal{B} : H^1_0(\Omega) \times H^1_0(\Omega) \to \mathbb{R}$ and $\mathcal{F} : H^1_0(\Omega) \to \mathbb{R}$ denote the bilinear and linear forms respectively defined by

$$\mathcal{B}(u, v) = \int_\Omega (\boldsymbol{\nabla} u \cdot \boldsymbol{\nabla} v + \kappa^2 uv)\,\mathrm{d}\boldsymbol{x}; \quad \mathcal{F}(v) = \int_\Omega fv\,\mathrm{d}\boldsymbol{x}. \tag{7}$$

The corresponding forms defined over an individual element $K \in \mathcal{P}$ as opposed to the whole of Ω are denoted by $\mathcal{B}_K(\cdot,\cdot)$ and $\mathcal{F}_K(\cdot)$ respectively. Likewise, the global energy norm $|\!|\!|\cdot|\!|\!|$ is defined by $|\!|\!|v|\!|\!|^2 = \mathcal{B}(v, v)$ while the corresponding local quantity is denoted by $|\!|\!|\cdot|\!|\!|_K$. The same convention is adopted for other norms such as the L_2-norm $\|\cdot\|$.

3. A Posteriori Error Estimation

We now turn our attention to the construction of robust a posteriori estimators for the error $e = u - \mathrm{u}_{\mathcal{P}}$ in the finite element approximation. This problem was also considered in [2] where it was observed that one of the key ingredients in developing robust bounds is the construction of an appropriate set of boundary flux functions $\{g_K : K \in \mathcal{P}\}$ on each of the element edges satisfying the consistency condition

$$g_K + g_{K'} = 0 \text{ on } \partial K \cap \partial K'. \tag{8}$$

These functions were then used as Neumann boundary data for a local boundary value problem of the form (1) with source term given by the local residual $r_{\mathcal{P}} = f + \Delta\,\mathrm{u}_{\mathcal{P}} - \kappa^2\,\mathrm{u}_{\mathcal{P}}$. The energy norms of the solutions of the local problems were shown to provide a guaranteed, robust upper bound on the error in the finite element approximation. Here, we adopt a similar approach with the important difference that it will not be necessary to introduce the infinite dimensional local boundary value problem. In fact, the estimator will be given *explicitly* in terms of readily available quantities involving the residual $r_{\mathcal{P}}$ and the difference $g_K - \boldsymbol{n}_K \cdot \mathbf{grad}\,\mathrm{u}_{\mathcal{P}|K}$ between the post-processed boundary fluxes and the flux in the finite element approximation.

We begin by briefly recalling the procedure for the construction of the boundary fluxes from [2] to which the reader is referred for further details.

3.1. **Construction of Inter-element Fluxes.** Let $\mathcal{N}$ denote the set of element vertices in the partition $\mathcal{P}$. For each $n \in \mathcal{N}$, let $\theta_n \in X_{\mathcal{P}}$ denote the Lagrange basis function characterized by the conditions $\theta_n(\boldsymbol{x}_m) = \delta_{nm}$ for all $m \in \mathcal{N}$ where δ_{nm} is the Kronecker symbol and let $\mathcal{P}_n$ denote the set of elements having a vertex at $\boldsymbol{x}_n$. Similarly, let $\mathcal{N}(\gamma) \subset \mathcal{N}$ denote the vertices of an element edge γ and define a set of piecewise linear functions $\{\psi_\gamma^m,\ m \in \mathcal{N}(\gamma)\}$ on the edge by the conditions

$$\int_\gamma \psi_\gamma^m \theta_n \,\mathrm{d}s = \delta_{mn}, \quad m, n \in \mathcal{N}(\gamma). \tag{9}$$

These functions are used to define the fluxes $\{g_K\}$ on the interfaces as follows. Each inter-element edge γ is assigned an arbitrary (but fixed) orientation by choosing a unique normal vector $\boldsymbol{n}$ on the interface. We define a piecewise constant function $\sigma_K : \partial K \to \{+1, -1\}$ by the rule $\sigma_K = 1$ on γ if $\boldsymbol{n}_K = \boldsymbol{n}$ on γ and $\sigma_K = -1$ otherwise. The flux approximation on an interface γ of element K is written in the form

$$g_K = \left\langle \frac{\partial \,\mathrm{u}_{\mathcal{P}}}{\partial \boldsymbol{n}_K} \right\rangle + \sigma_K \sum_{m \in \mathcal{N}(\gamma)} \alpha_\gamma^m \psi_\gamma^m \tag{10}$$

where

$$\left\langle \frac{\partial \,\mathrm{u}_{\mathcal{P}}}{\partial \boldsymbol{n}_K} \right\rangle = \frac{1}{2} \boldsymbol{n}_K \cdot \left(\boldsymbol{\nabla} \,\mathrm{u}_{\mathcal{P}} \,\big|_K + \boldsymbol{\nabla} \,\mathrm{u}_{\mathcal{P}} \,\big|_{K'} \right)$$

is the average of the finite element approximation to the flux from the elements K and K' sharing the edge γ. This construction ensures the consistency condition (8) is automatically enforced.

If the coefficients $\{\alpha_\gamma^m,\ m \in \mathcal{N}(\gamma)\}$, satisfy the conditions

$$\forall n \in \mathcal{N} : - \sum_{\gamma \subset \partial K} \sigma_{K|\gamma} \sum_{m \in \mathcal{N}(\gamma)} \delta_{nm} \alpha_\gamma^m = \mathcal{D}_K \left(\theta_n \right) \quad \forall K \subset \mathcal{P}_n, \tag{11}$$

where

$$\mathcal{D}_K(v) = \mathcal{F}_K(v) - \mathcal{B}_K(\mathrm{u}_{\mathcal{P}}, v) + \int_{\partial K} \left\langle \frac{\partial \,\mathrm{u}_{\mathcal{P}}}{\partial \boldsymbol{n}_K} \right\rangle v \,\mathrm{d}s,$$

then $\{g_K\}$ are said to be *equilibrated fluxes* [3]. The conditions (11) represent a linear algebraic system on the patch $\mathcal{P}_n$. The system is analysed at length in [3] and shown to be singular but solvable nevertheless.

Unfortunately, as shown in [2], these equilibrated fluxes give rise to an error estimator which is not robust in the limit as $\kappa \to \infty$. Luckily, a simple remedy is given in [2]: replace the Lagrange basis function θ_n appearing in the conditions (11) with an appropriately modified function denoted by θ_n^* (see below) and solve the resulting equations (11) in a least squares sense.

We construct the function θ_n^* as follows. Let $K \in \mathcal{P}$ be a triangular element as shown in Figure 1 and suppose that the basis function θ_n corresponds to vertex $\boldsymbol{x}_3$. We define an auxiliary point $\boldsymbol{x}_P \in K$ by the expression $\boldsymbol{x}_P = \delta \boldsymbol{x}_1 + \delta \boldsymbol{x}_2 + (1 - 2\delta) \boldsymbol{x}_3$, where $\delta = \frac{1}{2} \min(1, 1/(\kappa \rho_K))$ and ρ_K is the inradius

of element K. We form a sub-mesh of the element K using the point $\boldsymbol{x}_P$ in K as shown in Figure 1. The function θ_n^* is defined to be the piecewise affine function relative to the sub-mesh with $\theta_n^*(\boldsymbol{x}_n) = 1$ and vanishing at remaining nodes (see Figure 1).

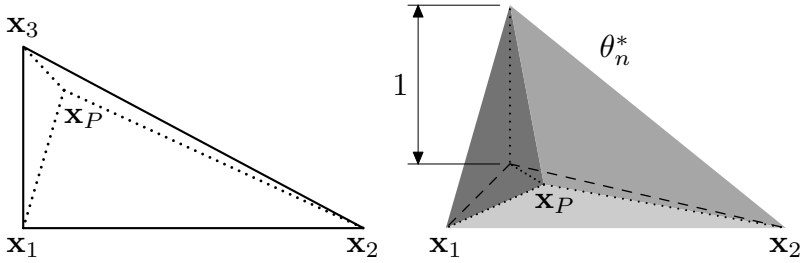

FIGURE 1. Construction of the approximate minimum energy extension θ_n^* on a triangle. The auxiliary point $\boldsymbol{x}_P$ has barycentric coordinates $(\delta, \delta, 1-2\delta)$, where $\delta = \frac{1}{2}\min(1, 1/(\kappa\rho_K))$. The submesh induced by the point $\boldsymbol{x}_P$ (left) and the piecewise linear graph of θ_n^* (right).

3.2. **A Posteriori Error Estimation.** Let $\mathbb{P}_1(K)$ denote the space of piecewise affine functions defined over an element K, and let $\Pi_K : L_2(K) \to \mathbb{P}_1(K)$ denote the orthogonal projector with respect to the usual inner product on $L_2(K)$.

Lemma 1. *Let $K \in \mathcal{P}$ be any element, $\{g_K\}$ be a set of fluxes satisfying the consistency condition* (8) *and $\boldsymbol{\Sigma}_K$ denote the set of vector fields on element K defined by*

$$\boldsymbol{\Sigma}_K = \{\boldsymbol{\tau} \in \boldsymbol{H}(\mathrm{div}, K) : \boldsymbol{n}_K \cdot \boldsymbol{\tau} = g_K \text{ on } \partial K\}. \tag{12}$$

For all choices of $\{\boldsymbol{\tau}_K\}_{K\in\mathcal{P}}$ such that $\boldsymbol{\tau}_K \in \boldsymbol{\Sigma}_K$, there holds

$$|\!|\!| e |\!|\!|^2 \leq \sum_{K\in\mathcal{P}} \left\{ \eta_K(\boldsymbol{\tau}_K) + \min\left(\frac{h_K}{\pi}, \frac{1}{\kappa}\right) \|f - \Pi_K f\|_K \right\}^2 \tag{13}$$

where $\eta_K : \boldsymbol{\Sigma}_K \to \mathbb{R}^+$ is defined by the rule

$$\eta_K(\boldsymbol{\tau})^2 = \|\boldsymbol{\tau} - \mathbf{grad}\, \mathrm{u}_\mathcal{P}\|_K^2 + \frac{1}{\kappa^2}\|\Pi_K f - \kappa^2\, \mathrm{u}_\mathcal{P} + \mathrm{div}\, \boldsymbol{\tau}\|_K^2.$$

Proof. The error $e = u - \mathrm{u}_\mathcal{P} \in H_0^1(\Omega)$ in the finite element approximation satisfies

$$\mathcal{B}(e, v) = \mathcal{F}(v) - \mathcal{B}(\mathrm{u}_\mathcal{P}, v) = \sum_{K\in\mathcal{P}} \left\{ \int_K f v \,\mathrm{d}\boldsymbol{x} + \int_{\partial K} g_K v \,\mathrm{d}s - \mathcal{B}_K(\mathrm{u}_\mathcal{P}, v) \right\}$$

for each $v \in H_0^1(\Omega)$, where condition (8) has been used along with the fact that the test function v has vanishing trace on the domain boundary. Let $\boldsymbol{\tau} \in \boldsymbol{\Sigma}_K$, then an application of the divergence theorem reveals that

$$\int_{\partial K} g_K v \,\mathrm{d}s = \int_K \boldsymbol{\tau} \cdot \mathbf{grad}\, v \,\mathrm{d}\boldsymbol{x} + \int_K v\, \mathrm{div}\, \boldsymbol{\tau} \,\mathrm{d}\boldsymbol{x}.$$

With the aid of this result, the term appearing in parentheses above may then be written as a sum of the quantities

$$\int_K \left(\Pi_K f - \kappa^2\, \mathrm{u}_{\mathcal{P}} + \operatorname{div} \boldsymbol{\tau}\right) v \,\mathrm{d}\boldsymbol{x} + \int_K (\boldsymbol{\tau} - \mathbf{grad}\, \mathrm{u}_{\mathcal{P}}) \cdot \mathbf{grad}\, v \,\mathrm{d}\boldsymbol{x}$$

and

$$\int_K (f - \Pi_K f)\, v \,\mathrm{d}\boldsymbol{x}.$$

Straightforward applications of the Cauchy-Schwarz inequality may be used to show that the former quantity is bounded by

$$\|\Pi_K f - \kappa^2\, \mathrm{u}_{\mathcal{P}} + \operatorname{div} \boldsymbol{\tau}\|_K \|v\|_K + \|\boldsymbol{\tau} - \mathbf{grad}\, \mathrm{u}_{\mathcal{P}}\|_K \|\mathbf{grad}\, v\|_K$$

which is in turn bounded by $\eta_K(\boldsymbol{\tau})\, |\!|\!| v |\!|\!|_K$ by again using the Cauchy-Schwarz inequality.

The remaining quantity is treated slightly differently depending on the magnitude of κ. The Cauchy-Schwarz inequality may be used to derive the simple bound

$$\int_K (f - \Pi_K f)\, v \,\mathrm{d}\boldsymbol{x} \leq \|f - \Pi_K f\|_K \|v\|_K \leq \kappa^{-1} \|f - \Pi_K f\|_K\, |\!|\!| v |\!|\!|_K\,.$$

On the other hand, the definition of $\Pi_K f$ means that for any constant $c \in \mathbb{R}$, we have

$$\int_K (f - \Pi_K f)\, v \,\mathrm{d}\boldsymbol{x} = \int_K (f - \Pi_K f)\, (v - c)\, \,\mathrm{d}\boldsymbol{x} \leq \|f - \Pi_K f\|_K \|v - c\|_K,$$

which we then bound with the aid of the Poincaré inequality [9]

$$\inf_{c \in \mathbb{R}} \|v - c\|_K \leq \frac{h_K}{\pi} \|\mathbf{grad}\, v\|_K$$

to obtain the following alternative estimate

$$\int_K (f - \Pi_K f)\, v \,\mathrm{d}\boldsymbol{x} \leq \frac{h_K}{\pi} \|f - \Pi_K f\|_K\, |\!|\!| v |\!|\!|_K\,.$$

By combining this with the earlier estimate, we deduce that the following bound holds

$$\int_K (f - \Pi_K f)\, v \,\mathrm{d}\boldsymbol{x} \leq \min\left(\frac{h_K}{\pi}, \frac{1}{\kappa}\right) \|f - \Pi_K f\|_K\, |\!|\!| v |\!|\!|_K\,.$$

In summary, we have shown that

$$\mathcal{B}(e, v) \leq \sum_{K \in \mathcal{P}} \left\{ \eta_K(\boldsymbol{\tau}) + \min\left(\frac{h_K}{\pi}, \frac{1}{\kappa}\right) \|f - \Pi_K f\|_K \right\} |\!|\!| v |\!|\!|_K$$

and the proof is completed with a final application of the Cauchy-Schwarz inequality. □

Although our primary concern in the present paper is the case in which κ is non-zero, the result in Lemma 1 is also applicable to the more usual case considered in the literature when κ vanishes. Specifically, if the field $\boldsymbol{\tau}_K$ satisfies the additional constraint whereby $\Pi_K f - \kappa^2\, \mathrm{u}_{\mathcal{P}} + \operatorname{div} \boldsymbol{\tau}_K$ vanishes, then it is not difficult to modify the above proof to show that the estimate (13) then

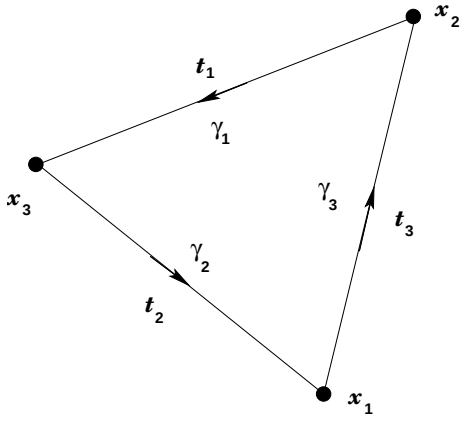

FIGURE 2. Notation for vertices, edges and tangent vectors of a general element K used in the construction of non-trivial flux fields $\boldsymbol{\tau} \in \boldsymbol{\Sigma}_K$.

holds with $\eta_K(\boldsymbol{\tau})$ reduced to $\|\boldsymbol{\tau}_K - \mathbf{grad}\, \mathrm{u}_{\mathcal{P}}\|_K$ and $\min(h_K/\pi, \kappa^{-1})$ reduced to h_K/π.

Lemma 1 is only of interest if one can establish that the sets $\boldsymbol{\Sigma}_K$ are non-empty. We present two alternative constructions for $\boldsymbol{\tau} \in \boldsymbol{\Sigma}_K$ where $K \in \mathcal{P}$ is an arbitrary element. For notational convenience, we assume that the vertices and edges of the triangle K are labelled as shown in Figure 2. In particular, we draw the reader's attention to the fact that $\boldsymbol{t}_1$, $\boldsymbol{t}_2$ and $\boldsymbol{t}_3$ denote the *actual tangent vectors* on the element edges rather than the unit tangent. We shall continue to use $\boldsymbol{n}$ to denote the unit outward pointing normal.

3.3. **Flux Construction #1.** We construct a flux function in the form

$$\boldsymbol{\tau}_K^{(1)} = \mathbf{grad}\, \mathrm{u}_{\mathcal{P}|K} + \boldsymbol{\tau}_K^L + \boldsymbol{\tau}_K^Q.$$

The vector field $\boldsymbol{\tau}_K^L$ is defined by

$$\boldsymbol{\tau}_K^L = \frac{1}{2|K|} \sum_{n \in \mathcal{N}(K)} \boldsymbol{\varrho}_n^{(K)} \lambda_n \tag{14}$$

where $|K|$ is the area of the element and

$$\begin{aligned}
\boldsymbol{\varrho}_1^{(K)} &= |\gamma_3| \left(g_K - \boldsymbol{n}_K \cdot \mathbf{grad}\, \mathrm{u}_{\mathcal{P}}\right)_{|\gamma_3}(\boldsymbol{x}_1)\boldsymbol{t}_2 \\
&\quad -|\gamma_2| \left(g_K - \boldsymbol{n}_K \cdot \mathbf{grad}\, \mathrm{u}_{\mathcal{P}}\right)_{|\gamma_2}(\boldsymbol{x}_1)\boldsymbol{t}_3 \\
\boldsymbol{\varrho}_2^{(K)} &= |\gamma_1| \left(g_K - \boldsymbol{n}_K \cdot \mathbf{grad}\, \mathrm{u}_{\mathcal{P}}\right)_{|\gamma_1}(\boldsymbol{x}_2)\boldsymbol{t}_3 \\
&\quad -|\gamma_3| \left(g_K - \boldsymbol{n}_K \cdot \mathbf{grad}\, \mathrm{u}_{\mathcal{P}}\right)_{|\gamma_3}(\boldsymbol{x}_2)\boldsymbol{t}_1 \\
\boldsymbol{\varrho}_3^{(K)} &= |\gamma_2| \left(g_K - \boldsymbol{n}_K \cdot \mathbf{grad}\, \mathrm{u}_{\mathcal{P}}\right)_{|\gamma_2}(\boldsymbol{x}_3)\boldsymbol{t}_1 \\
&\quad -|\gamma_1| \left(g_K - \boldsymbol{n}_K \cdot \mathbf{grad}\, \mathrm{u}_{\mathcal{P}}\right)_{|\gamma_1}(\boldsymbol{x}_3)\boldsymbol{t}_2
\end{aligned} \tag{15}$$

whilst $\boldsymbol{\tau}_K^Q$ is defined by

$$\boldsymbol{\tau}_K^Q = \frac{1}{3}\left(\beta_1 \boldsymbol{t}_1\boldsymbol{t}_1^T + \beta_2 \boldsymbol{t}_2\boldsymbol{t}_2^T + \beta_3 \boldsymbol{t}_3\boldsymbol{t}_3^T\right)\mathbf{grad}(\Pi_K f - \kappa^2\,\mathrm{u}_{\mathcal{P}})(\overline{\boldsymbol{x}}_K) \tag{16}$$

where $\overline{\boldsymbol{x}}_K$ denotes the centroid of element K, $\beta_1 = \lambda_2\lambda_3$ etc. and λ_1, λ_2, λ_3 denote the barycentric coordinates on the triangle K. It is easy to see that $\boldsymbol{\tau}_K^Q$ has vanishing normal components on each edge of element K whilst it is shown in [1, Lemma 6] that $\boldsymbol{\tau}_K^L$ satisfies $\boldsymbol{n}_K \cdot \boldsymbol{\tau}_K^L = g_K - \boldsymbol{n}_K \cdot \mathbf{grad}\,\mathrm{u}_{\mathcal{P}|K}$ on ∂K and, as consequence, $\boldsymbol{\tau}_K^{(1)} \in \boldsymbol{\Sigma}_K$.

Lemma 2. *If $K \in \mathcal{P}$ is any element for which $\kappa\rho_K \leq 1/\mathcal{C}_0$, where $\mathcal{C}_0$ is defined in* (5)*, then*

$$\eta_K(\boldsymbol{\tau}_K^{(1)}) \leq C\left\{|\!|\!|e|\!|\!|_{\widetilde{K}} + h_K\|f - \Pi f\|_{\widetilde{K}}\right\} \tag{17}$$

where the final term is defined by the following relation

$$\|f - \Pi f\|_{\widetilde{K}}^2 = \sum_{J\subset\widetilde{K}} \|f - \Pi_J f\|_J^2. \tag{18}$$

Proof. Observe that $\boldsymbol{\tau}_K^L$ has constant divergence over the element K whilst $\mathbf{grad}\,\mathrm{u}_{\mathcal{P}|K}$ has vanishing divergence over the element, and therefore

$$\operatorname{div}\boldsymbol{\tau}_K^L = \frac{1}{|K|}\int_{\partial K} \boldsymbol{n}_K \cdot \boldsymbol{\tau}_K^L\,\mathrm{d}s = \frac{1}{|K|}\int_{\partial K} g_K\,\mathrm{d}s.$$

Equally well, a simple computation reveals that $\operatorname{div}(\beta_1\boldsymbol{t}_1) = \lambda_2 - \lambda_3$ etc. and as a consequence,

$$\begin{aligned}
&-\operatorname{div}\boldsymbol{\tau}_K^Q \\
&\quad= \{(\boldsymbol{x}_1 - \overline{\boldsymbol{x}}_K)\lambda_1 + (\boldsymbol{x}_2 - \overline{\boldsymbol{x}}_K)\lambda_2 + (\boldsymbol{x}_3 - \overline{\boldsymbol{x}}_K)\lambda_3\} \cdot \mathbf{grad}(\Pi_K f - \kappa^2\,\mathrm{u}_{\mathcal{P}})(\overline{\boldsymbol{x}}_K) \\
&\quad= (\boldsymbol{x} - \overline{\boldsymbol{x}}_K) \cdot \mathbf{grad}(\Pi_K f - \kappa^2\,\mathrm{u}_{\mathcal{P}})(\overline{\boldsymbol{x}}_K).
\end{aligned}$$

The fact that $\Pi_K f - \kappa^2\,\mathrm{u}_{\mathcal{P}}$ is affine over the element may be exploited to rewrite this quantity in the alternative form

$$-\operatorname{div}\boldsymbol{\tau}_K^Q = (\Pi_K f - \kappa^2\,\mathrm{u}_{\mathcal{P}})(\boldsymbol{x}) - \frac{1}{|K|}\int_K \left(\Pi_K f - \kappa^2\,\mathrm{u}_{\mathcal{P}}\right)\,\mathrm{d}\boldsymbol{x}.$$

Moreover, the assumption $\kappa\rho_K \leq 1/\mathcal{C}_0$ means that all elements K' sharing a common edge or vertex with the element K satisfy $\kappa\rho_{K'} \leq \mathcal{C}_0\kappa\rho_K \leq 1$, and as a result, the functions θ^* defined in Section 3.1 coincide with the standard piecewise linear nodal functions. This means that the equilibration condition (11) is satisfied as an *equality* on element K and hence,

$$\int_{\partial K} g_K\,\mathrm{d}s = -\int_K \left(f - \kappa^2\,\mathrm{u}_{\mathcal{P}}\right)\,\mathrm{d}\boldsymbol{x} = -\int_K \left(\Pi_K f - \kappa^2\,\mathrm{u}_{\mathcal{P}}\right)\,\mathrm{d}\boldsymbol{x}$$

where the fact that $\Pi_K f$ is a projection has been used to obtain the second equality. Combining this with the earlier results, we conclude that

$$\operatorname{div}\boldsymbol{\tau}_K^{(1)} + \Pi_K f - \kappa^2\,\mathrm{u}_{\mathcal{P}} = 0 \text{ in } K. \tag{19}$$

This identity means that the second term appearing in $\eta_K(\boldsymbol{\tau}_K)$ vanishes when $\kappa\rho_K \leq 1/\mathcal{C}_0$.

We now turn our attention to the first term appearing in $\eta_K(\boldsymbol{\tau}_K)$. Using the first estimate on [1, Page 1795] gives

$$\|\boldsymbol{\tau}_K^L\|_K^2 \leq C \sum_{\gamma\in\partial K} |\gamma| \, \|g_K - \boldsymbol{n}_K \cdot \mathbf{grad}\, \mathrm{u}_\mathcal{P}\|_\gamma^2, \tag{20}$$

and hence, recalling that $\kappa\rho_K \leq 1/\mathcal{C}_0$ and using the triangle inequality in conjunction with estimates Lemma 5(2) and Lemma 6 of [2], we conclude that

$$\|\boldsymbol{\tau}_K^L\|_K \leq C \left\{ |\!|\!| e |\!|\!|_{\widetilde{K}} + h_K \|f - \Pi f\|_{\widetilde{K}} \right\}.$$

Similarly, using the triangle inequality and the relations $\|\beta_1\|_K = C|K|^{1/2}$ and $|\boldsymbol{t}_1| = |\gamma_1| \leq h_K$ etc., we find that

$$\|\boldsymbol{\tau}_K^Q\|_K \leq C h_K^2 \|\mathbf{grad}(\Pi_K f - \kappa^2\, \mathrm{u}_\mathcal{P})\|_K,$$

which, with the aid of an inverse estimate and the fact that $\mathbf{grad}\, \mathrm{u}_\mathcal{P}$ is constant, gives

$$\|\boldsymbol{\tau}_K^Q\|_K \leq C h_K \|\Pi_K f - \kappa^2\, \mathrm{u}_\mathcal{P}\|_K = C h_K \|\Pi_K r_\mathcal{P}\|_K$$

where $r_\mathcal{P} = f + \Delta\, \mathrm{u}_\mathcal{P} - \kappa^2\, \mathrm{u}_\mathcal{P}$. Applying the final estimate on [2, Page 343] and again recalling that $\kappa\rho_K \leq 1/\mathcal{C}_0$, we arrive at the conclusion

$$\|\boldsymbol{\tau}_K^Q\|_K \leq C \left\{ |\!|\!| e |\!|\!|_K + h_K \|f - \Pi_K f\|_K \right\}.$$

Applying the triangle inequality gives an estimate for $\|\boldsymbol{\tau}_K^{(1)} - \mathbf{grad}\, \mathrm{u}_\mathcal{P}\|_K$ in terms of $\|\boldsymbol{\tau}_K^L\|_K$ and $\|\boldsymbol{\tau}_K^Q\|_K$, which in conjunction with the foregoing results, produces the desired estimate for $\eta_K(\boldsymbol{\tau}_K^{(1)})$. □

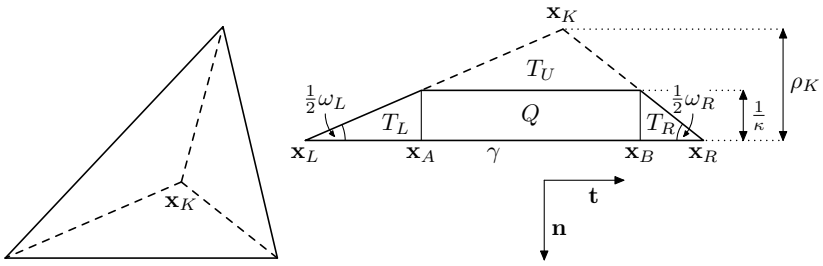

FIGURE 3. Sub-division of a triangle for the explicit construction of $\boldsymbol{\tau}_K^{(2)}$ (left), and sub-mesh used within each sub-element (right).

3.4. **Flux Construction #2.** We construct $\boldsymbol{\tau}_K^{(2)} \in \boldsymbol{\Sigma}_K$ in the form

$$\boldsymbol{\tau}_K^{(2)} = \mathbf{grad}\, \mathrm{u}_{\mathcal{P}|K} + \boldsymbol{\tau}_K^O \tag{21}$$

where $\boldsymbol{\tau}_K^O \in \boldsymbol{H}(\mathrm{div}, K)$ has normal components given by

$$\boldsymbol{n}_K \cdot \boldsymbol{\tau}_K^O = R_K^O = g_K - \boldsymbol{n}_K \cdot \mathbf{grad}\, \mathrm{u}_{\mathcal{P}|K}. \tag{22}$$

The vector field $\boldsymbol{\tau}_K^O$ itself is defined in a piecewise fashion based on a subdivision of the element K consisting of the three sub-triangles obtained by connecting the incentre $\boldsymbol{x}_K$ of the element to the vertices of K as shown in Figure 3 (left).

It suffices to describe the construction of $\boldsymbol{\tau}_K^O$ in the sub-triangle corresponding to a particular edge $\gamma \subset \partial K$ joining vertices $\boldsymbol{x}_L$ and $\boldsymbol{x}_R$ of the original element.

This sub-element is illustrated in Figure 3 (right) in the case when the element size satisfies $\rho_K \geq 1/\kappa$, in which case the sub-element is itself further subdivided into the union of triangles T_L, T_R, T_U and a rectangle Q corresponding to a line drawn parallel to, and at a distance $1/\kappa$ from, the edge γ. In the event that $\rho_K < 1/\kappa$, the rectangle Q and the upper triangle T_U vanishes and only the sub-triangles T_L and T_R remain.

The vector field $\boldsymbol{\tau}_K^O$ is then defined on the sub-element as follows using the notation given in Figure 3:

$$\boldsymbol{\tau}_K^O(\boldsymbol{x}) = \begin{cases} R^O_{K|\gamma}(\boldsymbol{x}_L)\lambda_L(\boldsymbol{x})\left(\boldsymbol{n} - \boldsymbol{t}\cot\frac{1}{2}\omega_L\right) + R^O_{K|\gamma}(\boldsymbol{x}_A)\lambda_A(\boldsymbol{x})\boldsymbol{n}, & \boldsymbol{x} \in T_L, \\ R^O_{K|\gamma}(\boldsymbol{x}_A + x\boldsymbol{t})(1-\kappa y)\boldsymbol{n}, & \boldsymbol{x} \in Q, \\ R^O_{K|\gamma}(\boldsymbol{x}_R)\lambda_R(\boldsymbol{x})\left(\boldsymbol{n} + \boldsymbol{t}\cot\frac{1}{2}\omega_R\right) + R^O_{K|\gamma}(\boldsymbol{x}_B)\lambda_B(\boldsymbol{x})\boldsymbol{n}, & \boldsymbol{x} \in T_R, \\ \boldsymbol{0} & \boldsymbol{x} \in T_U \end{cases} \tag{23}$$

where λ_L, λ_A, λ_R, and λ_B are the usual barycentric coordinates in T_L and T_R, $\boldsymbol{n}$ and $\boldsymbol{t}$ are unit vectors shown in Figure 3, and $x = (\boldsymbol{x}-\boldsymbol{x}_A)\cdot\boldsymbol{t}$ and $y = (\boldsymbol{x}_A-\boldsymbol{x})\cdot\boldsymbol{n}$ are the local Cartesian coordinates in Q. As before, in the case when $\rho_K < 1/\kappa$, the expressions for the rectangle Q and the upper triangle T_U are superfluous. It is readily verified that the vector field $\boldsymbol{\tau}_K^O$ has continuous (vanishing) normal components on interfaces of the sub-mesh and that the normal component on the element edge γ is given by $R^O_{K|\gamma}$. Consequently, $\boldsymbol{\tau}_K^{(2)} \in \boldsymbol{\Sigma}_K$.

The following property of the flux constructed above will prove useful later:

Lemma 3. *If $K \in \mathcal{P}$ is any element for which $\kappa\rho_K \geq 1/\mathcal{C}_0$, then*

$$\eta_K(\boldsymbol{\tau}_K^{(2)}) \leq C\left\{|\!|\!|e|\!|\!|_{\widetilde{K}} + \kappa^{-1}\|f - \Pi f\|_{\widetilde{K}}\right\}. \tag{24}$$

Proof. An elementary calculation using the definition of $\boldsymbol{\tau}_K^O$ reveals that

$$\|\boldsymbol{\tau}_K^O\|_Q^2 = \frac{1}{3}\kappa^{-1}\|R^O_{K|\gamma}\|^2_{L_2(\boldsymbol{x}_A,\boldsymbol{x}_B)}$$

and

$$\begin{aligned} \|\boldsymbol{\tau}_K^O\|^2_{T_L} &= \frac{1}{6}|T_L|\left\{R^O_{K|\gamma}(\boldsymbol{x}_L)^2\csc^2\frac{1}{2}\omega_L + R^O_{K|\gamma}(\boldsymbol{x}_L)R^O_{K|\gamma}(\boldsymbol{x}_A) + R^O_{K|\gamma}(\boldsymbol{x}_A)^2\right\} \\ &\leq C\kappa^{-1}\|R^O_{K|\gamma}\|^2_{L_2(\boldsymbol{x}_L,\boldsymbol{x}_A)} \end{aligned}$$

with a similar estimate for the contribution from T_R. These estimates, along with the triangle inequality, give

$$\|\boldsymbol{\tau}_K^{(2)} - \mathbf{grad}\,\mathrm{u}_{\mathcal{P}}\|_K^2 = \|\boldsymbol{\tau}_K^O\|_K^2 \leq C\kappa^{-1}\sum_{\gamma\subset\partial K}\|R^O_{K|\gamma}\|^2_\gamma. \tag{25}$$

Similarly, elementary computation reveals that

$$\operatorname{div}\boldsymbol{\tau}^O_{K|T_L} = \frac{1}{|T_L|}\int_{\boldsymbol{x}_A}^{\boldsymbol{x}_L} R_K^O\,\mathrm{d}\boldsymbol{x}, \quad \|\operatorname{div}\boldsymbol{\tau}_K^O\|^2_{T_L} \leq C\kappa\|R_K^O\|^2_{L_2(\boldsymbol{x}_L,\boldsymbol{x}_A)}$$

and

$$\operatorname{div} \boldsymbol{\tau}^O_{K|Q} = \kappa R^O_{K|\gamma}(\boldsymbol{x}_A + x\boldsymbol{t}), \quad \|\operatorname{div} \boldsymbol{\tau}^O_K\|^2_Q = \kappa \|R^O_K\|^2_{L_2(\boldsymbol{x}_A,\boldsymbol{x}_B)}.$$

These relations together with similar formulas on T_R imply

$$\|\operatorname{div} \boldsymbol{\tau}^O_K\|^2_K \leq C\kappa \|R^O_K\|^2_{\partial K}. \tag{26}$$

Observing that

$$\begin{aligned} \|\Pi_K f - \kappa^2 \,\mathrm{u}_{\mathcal{P}} + \operatorname{div} \boldsymbol{\tau}^{(2)}_K\|_K &\leq \|\Pi_K f - \kappa^2 \,\mathrm{u}_{\mathcal{P}}\|_K + \|\operatorname{div} \boldsymbol{\tau}^O_K\|_K \\ &= \|\Pi_K r_{\mathcal{P}}\|_K + \|\operatorname{div} \boldsymbol{\tau}^O_K\|_K, \end{aligned} \tag{27}$$

where we recall that $r_{\mathcal{P}} = f - \kappa^2 \,\mathrm{u}_{\mathcal{P}} + \Delta \,\mathrm{u}_{\mathcal{P}}$, and using the previous inequality along with the final estimate of [2, p. 343], we deduce that

$$\begin{aligned} &\kappa^{-1}\|\Pi_K f - \kappa^2 \,\mathrm{u}_{\mathcal{P}} + \operatorname{div} \boldsymbol{\tau}^{(2)}_K\|_K \leq \\ &\quad C\left\{\kappa^{-1}\min(h_K,\kappa^{-1})^{-1}\,|\!|\!|e|\!|\!|_K + \kappa^{-1}\|f - \Pi_K f\|_K + \kappa^{-1/2}\|R^O_K\|_{L_2(\partial K)}\right\}. \end{aligned}$$

Combining this with the earlier estimate for $\|\boldsymbol{\tau}^O_K\|_K$ gives

$$\begin{aligned} &\eta_K(\boldsymbol{\tau}^{(2)}_K) \leq \\ &\quad C\left\{\kappa^{-1}\min(h_K,\kappa^{-1})^{-1}\,|\!|\!|e|\!|\!|_K + \kappa^{-1}\|f - \Pi_K f\|_K + \kappa^{-1/2}\|R^O_K\|_{L_2(\partial K)}\right\}. \end{aligned}$$

Finally, using the triangle inequality and estimates [2, Lemma 5(2)] and [2, Lemma 6] leads to

$$\|R^O_K\|_{L_2(\partial K)} \leq C\min(h_K,\kappa^{-1})^{-1/2}\,|\!|\!|e|\!|\!|_{\widetilde{K}} + C\min(h_K,\kappa^{-1})^{1/2}\|f - \Pi f\|_{\widetilde{K}},$$

and inserting this estimate into the previous inequality and again using the fact that $\kappa\rho_K \geq 1/\mathcal{C}_0$ gives the claimed result. □

3.5. **A Posteriori Error Estimator.** Let $\boldsymbol{\tau}^{(1)}_K$, $\boldsymbol{\tau}^{(2)}_K \in \boldsymbol{\Sigma}_K$ denote the vector fields constructed above, and let $\boldsymbol{E}_K \in \mathbb{R}^{2\times 2}$ denote the symmetric matrix whose entries are given by

$$\begin{aligned} [\boldsymbol{E}_K]_{ij} &= \left(\boldsymbol{\tau}^{(i)}_K - \mathbf{grad}\,\mathrm{u}_{\mathcal{P}}, \boldsymbol{\tau}^{(j)}_K - \mathbf{grad}\,\mathrm{u}_{\mathcal{P}}\right)_K \\ &+ \frac{1}{\kappa^2}\left(\Pi_K f - \kappa^2\,\mathrm{u}_{\mathcal{P}} + \operatorname{div}\boldsymbol{\tau}^{(i)}_K, \Pi_K f - \kappa^2\,\mathrm{u}_{\mathcal{P}} + \operatorname{div}\boldsymbol{\tau}^{(j)}_K\right)_K \end{aligned} \tag{28}$$

for $1 \leq i, j \leq 2$.

We are now in a position to present our main result:

Theorem 1. *Let $\boldsymbol{E}_K$, $K \in \mathcal{P}$ denote the matrix defined in* (28)*. Then, there exists $\boldsymbol{\tau}^*_K \in \boldsymbol{\Sigma}_K$ such that*

$$\eta_K(\boldsymbol{\tau}^*_K) = \begin{cases} \dfrac{1}{\sqrt{\vec{1}^T \boldsymbol{E}_K^{-1}\vec{1}}} & \text{if } \boldsymbol{E}_K \text{ is non-singular,} \\ \dfrac{1}{\kappa}\|\Pi_K f - \kappa^2\,\mathrm{u}_{\mathcal{P}}\|_K & \text{otherwise,} \end{cases} \tag{29}$$

where $\vec{1} = [1,1]^T$. *Consequently, the error in the finite element approximation is bounded by*

$$\|\!|e|\!\|^2 \leq \sum_{K\in\mathcal{P}} \left\{ \eta_K(\boldsymbol{\tau}_K^*) + \min\left(\frac{h_K}{\pi}, \frac{1}{\kappa}\right) \|f - \Pi_K f\|_K \right\}^2 . \tag{30}$$

Moreover, there exists a positive constant C, *independent of any mesh-size or* κ, *such that*

$$\eta_K(\boldsymbol{\tau}_K^*) \leq \min\left(\eta_K(\boldsymbol{\tau}_K^{(1)}), \eta_K(\boldsymbol{\tau}_K^{(2)})\right) \leq C\left\{ \|\!|e|\!\|_{\widetilde{K}} + \min(h_K, \kappa^{-1}) \|f - \Pi f\|_{\widetilde{K}} \right\}. \tag{31}$$

The a posteriori error estimator suggested by this result involves the quantity $\vec{1}^T \boldsymbol{E}_K^{-1} \vec{1}$ which is a real number that may be readily computed in terms of the flux functions defined in the previous section and the local element residual. In particular, we emphasise that it is *not* necessary to construct the field $\boldsymbol{\tau}_K^*$ in the computer program since we only require the value of $\eta(\boldsymbol{\tau}_K^*)$ which is given explicitly in terms of the matrix $\boldsymbol{E}_K$. Moreover, the computation of the quantity involves only local computations over each element (the equilibrated fluxes are also obtained using computations over local patches).

At first glance, the error estimator may appear slightly unusual in comparison with standard existing error estimators, but may nevertheless be readily used to obtain a guaranteed upper bound on the error in the finite element approximation. Furthermore, the second estimate shows that the estimate is robust in both the limit as the element size $h_K \to 0$ and as $\kappa \to \infty$, provided that the additional data oscillation terms involving the (generally higher order) quantity $\|f - \Pi_K f\|_K$ may be neglected.

Proof. Let $K \in \mathcal{P}$. If the matrix $\boldsymbol{E}_K$ is non-singular, then $\boldsymbol{E}_K$ is symmetric, positive definite. If α_1, $\alpha_2 \in \mathbb{R}$ satisfy $\alpha_1 + \alpha_2 = 1$, then $\alpha_1 \boldsymbol{\tau}_K^{(1)} + \alpha_2 \boldsymbol{\tau}_K^{(2)} \in \boldsymbol{\Sigma}_K$ and Lemma 1 means that $\eta_K(\alpha_1 \boldsymbol{\tau}_K^{(1)} + \alpha_2 \boldsymbol{\tau}_K^{(2)})$ may be used to provide an upper bound on the error for all such choices of α_1 and α_2. It is easily verified in this case that

$$\eta_K(\alpha_1 \boldsymbol{\tau}_K^{(1)} + \alpha_2 \boldsymbol{\tau}_K^{(2)})^2 = \vec{\alpha}^T \boldsymbol{E}_K \vec{\alpha}$$

where $\vec{\alpha} = (\alpha_1, \alpha_2)$. Minimising the above quantity subject to the constraint $\vec{\alpha}^T \vec{1} = 1$ leads to the conclusion

$$\min_{\alpha_1+\alpha_2=1} \eta_K(\alpha_1 \boldsymbol{\tau}_K^{(1)} + \alpha_2 \boldsymbol{\tau}_K^{(2)}) = \left(\vec{1}^T \boldsymbol{E}_K^{-1} \vec{1}\right)^{-1/2}$$

and we may choose $\boldsymbol{\tau}_K^* = \alpha_1 \boldsymbol{\tau}_K^{(1)} + \alpha_2 \boldsymbol{\tau}_K^{(2)}$. The upper bound on the error in the finite element approximation now follows directly from Lemma 1 in conjunction with this choice of $\boldsymbol{\tau}_K^*$. A simple consequence of this minimisation process (choose $\alpha_1 = 1$ and $\alpha_2 = 0$, and apply Lemma 2) is that if $\kappa \rho_K \leq 1/\mathcal{C}_0$, then

$$\left(\vec{1}^T \boldsymbol{E}_K^{-1} \vec{1}\right)^{-1/2} \leq \eta_K(\boldsymbol{\tau}_K^{(1)}) \leq C\left\{ \|\!|e|\!\|_{\widetilde{K}} + h_K \|f - \Pi f\|_{\widetilde{K}} \right\},$$

whilst if $\kappa \rho_K > 1/\mathcal{C}_0$, then (choose $\alpha_1 = 0$ and $\alpha_2 = 1$, and apply Lemma 3)

$$\left(\vec{1}^T \boldsymbol{E}_K^{-1} \vec{1}\right)^{-1/2} \leq \eta_K(\boldsymbol{\tau}_K^{(2)}) \leq C\left\{ \|\!|e|\!\|_{\widetilde{K}} + \kappa^{-1} \|f - \Pi f\|_{\widetilde{K}} \right\}.$$

If the matrix $\boldsymbol{E}_K$ is singular, then Lemma 4 (proved below) shows that $g_K = \boldsymbol{n}_K \cdot \mathbf{grad}\, \mathrm{u}_{\mathcal{P}|K}$ on ∂K and $\Pi_K f - \kappa^2\, \mathrm{u}_{\mathcal{P}}$ is constant over the element. As a consequence $\mathbf{grad}\, \mathrm{u}_{\mathcal{P}|K} = \boldsymbol{\tau}_K^{(1)} = \boldsymbol{\tau}_K^{(2)} \in \boldsymbol{\Sigma}_K$ and we may choose $\boldsymbol{\tau}_K^*$ to be the gradient of the finite element approximation itself. It is easy to see that

$$\eta_K(\boldsymbol{\tau}_K^*) = \kappa^{-1} \|\Pi_K f - \kappa^2\, \mathrm{u}_{\mathcal{P}}\|_K$$

and, thanks to Lemmas 2 and 3,

$$\eta_K(\boldsymbol{\tau}_K^*) \le C \left\{ |\!|\!| e |\!|\!|_{\widetilde{K}} + \min(h_K, \kappa^{-1}) \|f - \Pi f\|_{\widetilde{K}} \right\}.$$

Combining the above estimates completes the proof. □

We conclude this section with a proof of the following result that was used in the proof of Theorem 1:

Lemma 4. *Let $K \in \mathcal{P}$ be any element. The matrix $\boldsymbol{E}_K$ defined in* (28) *is singular if and only if*

$$(a) \qquad g_K = \boldsymbol{n}_K \cdot \mathbf{grad}\, \mathrm{u}_{\mathcal{P}|K} \ \text{ on } \partial K$$
$$(b) \qquad \Pi_K f - \kappa^2\, \mathrm{u}_{\mathcal{P}} \ \text{ is constant in } K.$$

Proof. If (a) does not hold then $\boldsymbol{\tau}_K^L$ and $\boldsymbol{\tau}_K^O$ are non-zero and therefore linearly independent (by construction). In turn, this means that $\boldsymbol{\tau}_K^{(1)} - \mathbf{grad}\, \mathrm{u}_{\mathcal{P}|K}$ and $\boldsymbol{\tau}_K^{(2)} - \mathbf{grad}\, \mathrm{u}_{\mathcal{P}|K}$ are linearly independent and it follows that for all $\vec{\alpha} = (\alpha_1, \alpha_2) \in \mathbb{R}^2$:

$$\vec{\alpha}^T \boldsymbol{E}_K \vec{\alpha} \ge \|\alpha_1(\boldsymbol{\tau}_K^{(1)} - \mathbf{grad}\, \mathrm{u}_{\mathcal{P}|K}) + \alpha_2(\boldsymbol{\tau}_K^{(2)} - \mathbf{grad}\, \mathrm{u}_{\mathcal{P}|K})\|_K^2 \ge 0$$

with equality if and only if $\alpha_1 = \alpha_2 = 0$, and hence $\boldsymbol{E}_K$ is symmetric, positive definite. If (a) holds but (b) is violated, then $\boldsymbol{\tau}_K^L = \boldsymbol{\tau}_K^O = \mathbf{0}$ whilst $\boldsymbol{\tau}_K^Q$ is non-zero. Consequently,

$$\vec{\alpha}^T \boldsymbol{E}_K \vec{\alpha} = \alpha_1^2 \|\boldsymbol{\tau}_K^Q\|_K^2 + \kappa^{-2} \|\alpha_1 \operatorname{div} \boldsymbol{\tau}_K^Q + (\alpha_1 + \alpha_2)(\Pi_K f - \kappa^2\, \mathrm{u}_{\mathcal{P}})\|_K^2 \ge 0$$

with equality if and only if $\alpha_1 = \alpha_2 = 0$, and $\boldsymbol{E}_K$ is again symmetric, positive definite. In view of the fact that a symmetric, positive definite matrix is non-singular, these results show that if $\boldsymbol{E}_K$ is singular, then both (a) and (b) must hold. The proof of the reverse implication is simple: If both (a) and (b) hold, then $\boldsymbol{\tau}_K^L = \boldsymbol{\tau}_K^O = \boldsymbol{\tau}_K^Q = \mathbf{0}$. As a result, $\boldsymbol{\tau}_K^{(1)}$ and $\boldsymbol{\tau}_K^{(2)}$ coincide and it immediately follows from (28) that $\boldsymbol{E}_K$ is singular. □

4. Numerical Examples

We illustrate the performance of the estimators described above in the case of a problem with a smooth solution and a problem with a boundary layer.

Example 1. Consider the model problem (1) with data chosen to be $f(x, y) = \cos(\pi x)\cos(\pi y)$ on a square $\Omega = (-1/2, 1/2)^2$. The true solution is given by $u(x, y) = \cos(\pi x)\cos(\pi y)/(2\pi^2 + \kappa^2)$. Although the solution is smooth, it was found in [2] that it was precisely this kind of solution that caused existing a posteriori estimators to exhibit non-robust behaviour.

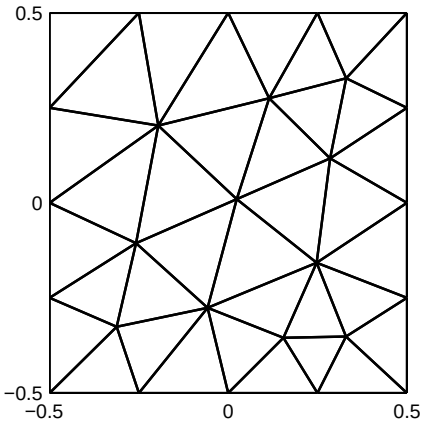

FIGURE 4. The mesh used in Example 1.

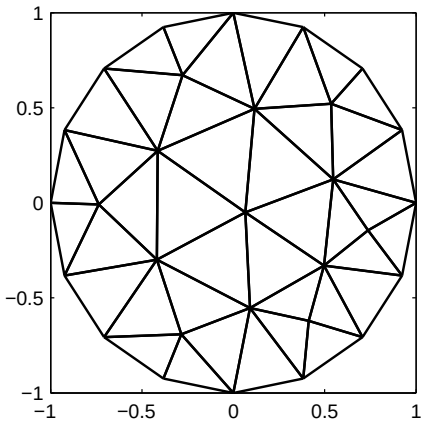

FIGURE 5. The mesh used in Example 2.

Example 2. Consider the model problem (1) with data chosen to be $f(x, y) = 1$ on a circle $\Omega = \{(x, y) : x^2 + y^2 < 1\}$. The circular domain was approximated by the regular polyhedron with 16 edges and an initial mesh with 40 triangles as depicted in Figure 5. The true solution can be expressed in terms of the modified Bessel function I_0 as $u(x, y) = \kappa^{-2}\,(1 - I_0(\kappa r)/I_0(\kappa))$, $\kappa \neq 0$ with $r = (x^2+y^2)^{1/2}$, and exhibits a steep layer in the neighbourhood of the boundary for larger values of κ, whilst $u(x, y) \to (1 - r^2)/4$ as $\kappa \to 0$.

We begin by considering the behaviour of the estimators in the case of Example 1, as the parameter κ is varied on a fixed mesh consisting of 36 triangles shown in Figure 4. The results obtained are shown in Figure 6 and Table 1. It will be observed that all estimators provided a guaranteed upper bound on the actual error as predicted in Lemma 1. Moreover, the estimator $\{\eta(\boldsymbol{\tau}_K^{(1)}) : K \in \mathcal{P}\}$ based on the first flux construction scheme is, as predicted in Lemma 2 robust in the limit as κ becomes small but degenerates sharply as κ grows. Conversely, the estimator $\{\eta(\boldsymbol{\tau}_K^{(2)}) : K \in \mathcal{P}\}$ based on the second flux construction scheme is robust in the limit as κ grows but degenerates sharply as $\kappa \to 0$ (and is undefined when κ vanishes). It is apparent that neither estimator can be used in isolation and expected to remain robust over the full range of κ.

Fortunately, Theorem 1 indicates that the minimum of these estimators can be taken as the estimator, and moreover, that the resulting estimator will not only be a guaranteed upper bound but will be robust over the full range of κ. The numerical results confirm the correctness of this result. In addition, Theorem 1 indicates that the estimator $\{\eta(\boldsymbol{\tau}_K^{*}) : K \in \mathcal{P}\}$ will also be a robust upper bound on the error that is at least as good as the one obtained taking the minimum. The numerical results also bear out this prediction with the optimised estimator providing a marginal improvement over the bulk of the range of values of κ with, as expected, the greatest improvement occurring in the transition where $\kappa h \approx 1$.

The corresponding results obtained for Example 2 are shown in Figure 7 and Table 2 from which similar conclusions can be drawn.

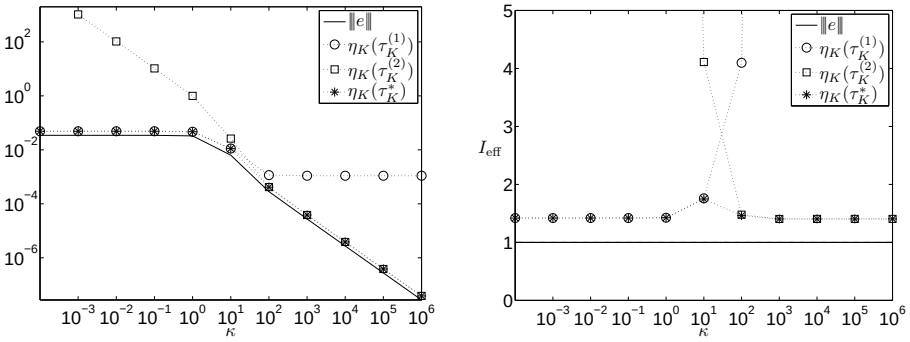

FIGURE 6. Variation of the error estimators (left) and their effectivity indices (right) versus κ on the fixed mesh shown in Figure 4 for Example 1.

κ	$\eta(\tau^{(1)})$	$\eta(\tau^{(2)})$	$\eta(\tau^*)$
0	1.419	—	1.419
10^{-3}	1.419	3.024×10^4	1.419
10^{-2}	1.419	3.024×10^3	1.419
10^{-1}	1.419	3.025×10^2	1.419
1	1.425	3.043×10^1	1.425
10	1.760	4.110	1.749
10^2	4.097	1.478	1.461
10^3	4.007×10^1	1.403	1.403
10^4	4.001×10^2	1.404	1.404
10^5	4.000×10^3	1.405	1.405
10^6	4.000×10^4	1.405	1.405

TABLE 1. Variation of effectivity indices for the error estimators versus κ on the fixed mesh shown in Figure 4 for Example 1.

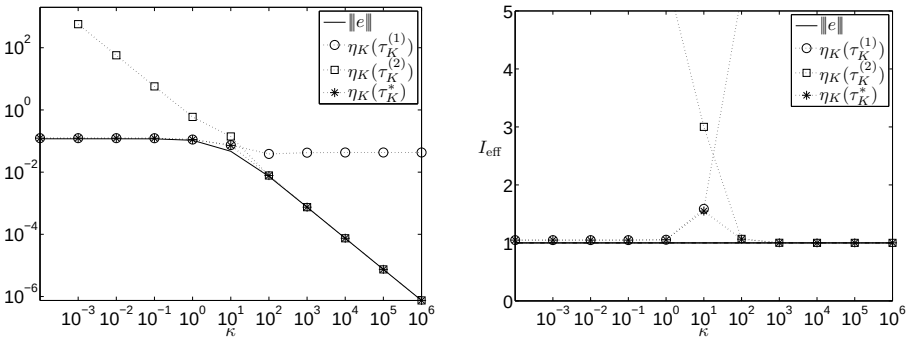

FIGURE 7. Variation of the error estimators (left) and their effectivity indices (right) versus κ on the fixed mesh shown in Figure 5 for Example 2.

In Figure 8, we present the results obtained when Example 1 is solved using uniform mesh refinement procedure in the case where $\kappa = 100$. Again, it is observed that neither of the estimators $\{\eta(\boldsymbol{\tau}_K^{(1)}) : K \in \mathcal{P}\}$ and $\{\eta(\boldsymbol{\tau}_K^{(2)}) : K \in \mathcal{P}\}$

κ	$\eta(\tau^{(1)})$	$\eta(\tau^{(2)})$	$\eta(\tau^*)$
0	1.047	—	1.047
10^{-3}	1.047	4.863×10^3	1.047
10^{-2}	1.047	4.863×10^2	1.047
10^{-1}	1.047	4.867×10^1	1.047
1	1.054	5.629	1.054
10	1.587	3.001	1.548
10^2	5.281	1.069	1.064
10^3	5.665×10^1	1.002	1.002
10^4	5.735×10^2	1.000	1.000
10^5	5.743×10^3	1.000	1.000
10^6	5.743×10^4	1.000	1.000

TABLE 2. Variation of effectivity indices for the error estimators versus κ on the fixed mesh shown in Figure 5 for Example 2.

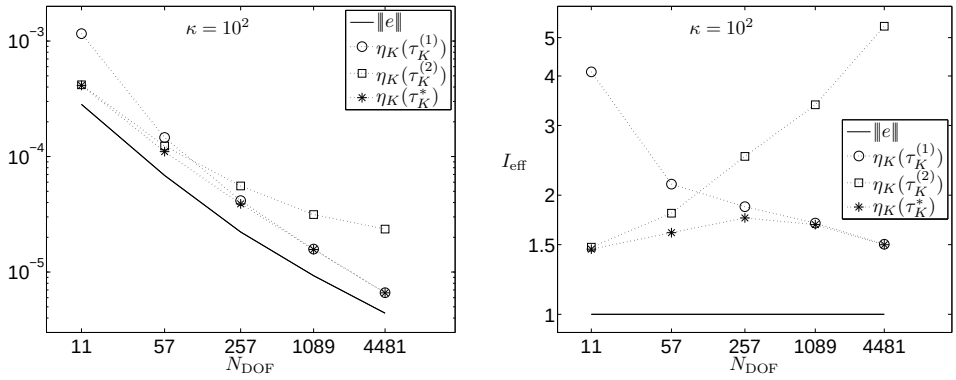

FIGURE 8. Behaviour of a posteriori error estimators (left) and effectivity indices (right) versus number of degrees of freedom N_{DOF} obtained for uniform refinement of Example 1 starting from mesh shown in Figure 4 in the case $\kappa = 100$.

is robust across the full range of mesh sizes. However, as predicted by Theorem 1, the minimum of the two estimators is robust and delivers guaranteed upper bounds across the full range. Once again, the optimised estimator $\{\eta(\boldsymbol{\tau}_K^*) : K \in \mathcal{P}\}$ provides a robust, guaranteed upper bound that behaves better across the ranges of values at which the transition in behaviour of the pure estimators occurs.

The presence of the steep boundary layer in the true solution for Example 2 suggests the use of an adaptive refinement procedure will be beneficial for this problem. We illustrate the behaviour of the estimators and investigate their suitability for guiding an adaptive refinement algorithm by applying a standard adaptive procedure. Starting from the mesh shown in Figure 5, all elements on which the local error estimator exceeds 50% of the largest local error estimator are refined at each step. The results obtained in the case when $\kappa = 100$ are shown in Figures 9 and 10.

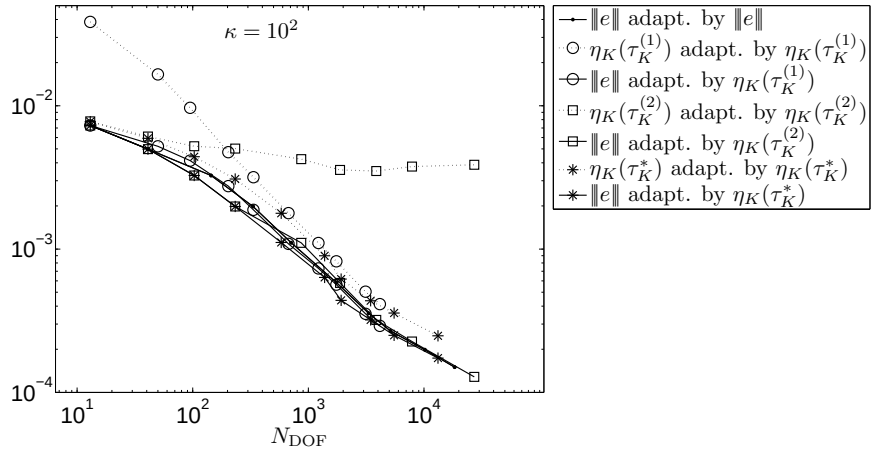

FIGURE 9. Convergence curves obtained using adaptive refinement procedure to solve Example 2 with $\kappa = 100$. Estimated errors (dotted lines) and true errors (solid lines) are shown when the adaptivity is driven by each of the estimators and by the true error.

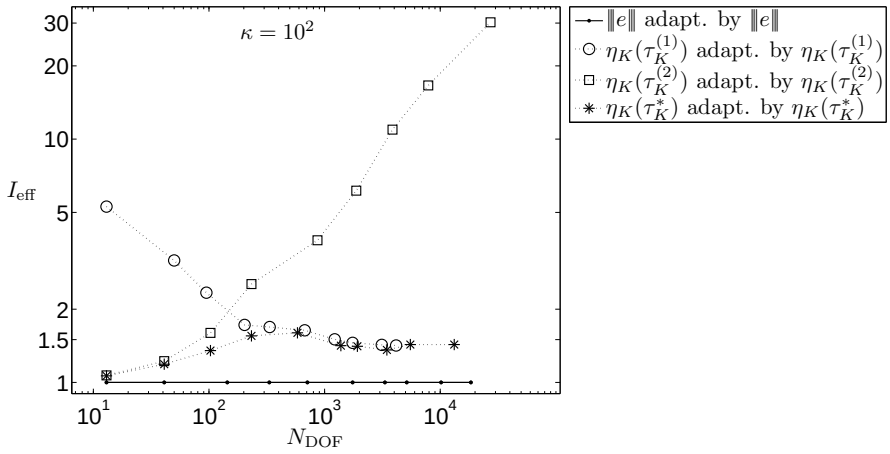

FIGURE 10. Effectivity of estimators using adaptive refinement procedure to solve Example 2 with $\kappa = 100$.

For comparison we run the adaptive algorithm guided by the true error (solid line with dots) and the various estimators: $\eta_K(\boldsymbol{\tau}_K^{(1)})$ (circles); $\eta_K(\boldsymbol{\tau}_K^{(2)})$ (squares) and $\eta_K(\boldsymbol{\tau}_K^{*})$ (asterisks). A cursory examination suggests that the actual convergence curves are relatively insensitive to the choice of estimator (or even the true error) used to drive the adaptive refinements. However, a closer examination of the figure shows that the estimator based on $\eta_K(\boldsymbol{\tau}_K^{*})$ produces the best results, with those obtained using the estimator $\eta_K(\boldsymbol{\tau}_K^{(2)})$ running a close second. The estimator based on $\eta_K(\boldsymbol{\tau}_K^{(1)})$ produces noticeably poorer accuracy on meshes in the transition region in which the robustness of the estimators changes. The

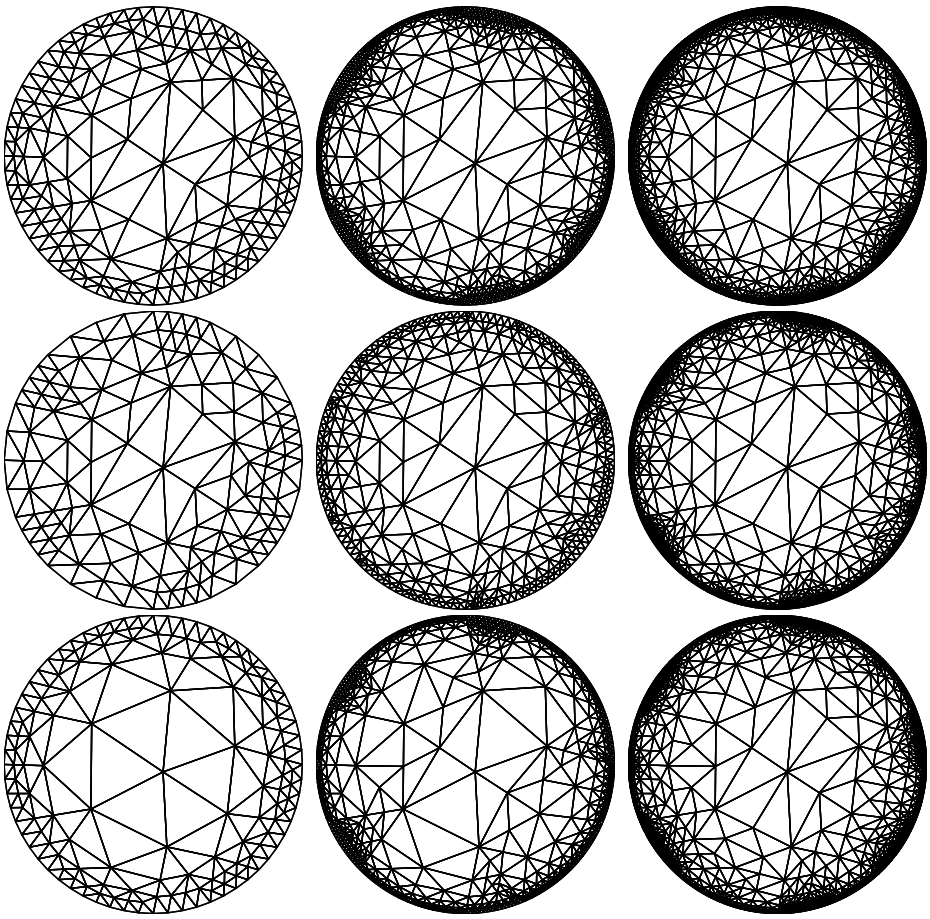

FIGURE 11. Adaptive meshes obtained using adaptive refinement procedure to solve Example 2 with $\kappa = 100$. Meshes arising in the 3rd, 5th and 7th adaptive step are shown in the columns, whilst rows 1–3 correspond to adaptivity driven by the true error, $\eta_K(\boldsymbol{\tau}_K^{(1)})$, and $\eta_K(\boldsymbol{\tau}_K^*)$ respectively.

meshes produced by the adaptive refinement procedures are shown in Figure 11. The meshes obtained using $\eta_K(\boldsymbol{\tau}_K^{(2)})$ are virtually identical to those obtained using $\eta_K(\boldsymbol{\tau}_K^*)$ and are therefore not shown. It will be observed that the meshes produced using the estimator $\eta_K(\boldsymbol{\tau}_K^{(1)})$ tend to exhibit a more diffuse refinement in the boundary layer compared with those obtained using the true error and the remaining estimators, which accounts for the poorer accuracy of the resulting approximation.

REFERENCES

[1] M. AINSWORTH, *A posteriori error estimation for discontinuous Galerkin finite element approximation*, SIAM J. Numer. Anal. 45 (2007) 1777–1798.

[2] M. Ainsworth and I. Babuška, *Reliable and robust a posteriori error estimation for singularly perturbed reaction diffusion problems*, SIAM J. Numer. Anal. 36 (1999) 331–353.
[3] M. Ainsworth and J.T. Oden, *A posteriori error estimation in finite element analysis*, Wiley-Interscience, New York, 2000.
[4] I. Cheddadi, R. Fučík, M.I. Prieto, and M. Vohralík, *Guaranteed and robust a posteriori error estimates for singularly perturbed reaction-diffusion problems*, to appear in M2AN Math. Model. Numer. Anal., DOI 10.1051/m2an/2009012, 2009.
[5] W. Dörfler, *A convergent adaptive algorithm for Poisson's equation*, SIAM J. Numer. Anal. 33 (1996) 1106–1124.
[6] S. Grosman, *An equilibrated residual method with a computable error approximation for a singularly perturbed reaction-diffusion problem on anisotropic finite element meshes*, M2AN Math. Model. Numer. Anal. 40 (2006) 239–267.
[7] P. Morin, R. Nochetto, and K. Siebert, *Data oscillation and convergence of adaptive FEM*, SIAM J. Numer. Anal. 38 (2000) 466–488.
[8] P. Neittaanmäki and S. Repin, *Reliable methods for computer simulation. Error control and a posteriori estimates*, Elsevier, Amsterdam, 2004.
[9] L.E. Payne and H.F. Weinberger, *An optimal Poincaré inequality for convex domains*, Arch. Rational Mech. Anal. 5 (1960) 286–292.
[10] H.-G. Roos, M. Stynes, and L. Tobiska, *Numerical Methods for Singularly Perturbed Differential Equations*, vol. 24 of Series in Computational Mathematics, Springer-Verlag, 1996.
[11] R. Stevenson, *Optimality of a standard adaptive finite element method*, Found. Comput. Math. 7 (2007) 245–269.
[12] R. Verfürth, *Robust a posteriori error estimators for a singularly perturbed reaction-diffusion equation*, Numer. Math. 78 (1998) 479–493.

Mark Ainsworth, Department of Mathematics, Strathclyde University, 26 Richmond St., Glasgow G1 1XH, Scotland.
E-mail address: M.Ainsworth@strath.ac.uk

Tomáš Vejchodský, Institute of Mathematics, Academy of Sciences, Žitná 25, CZ-115 67 Prague 1, Czech Republik.
E-mail address: vejchod@math.cas.cz